Journal of Molecular Structure 1249 (2022) 131640

Contents lists available at ScienceDirect

Journal of Molecular Structure

journal homepage: www.elsevier.com/locate/molstr

A cross-phase reaction coordinate in the formation of a simple copper (II) orotate complex: Lability of crystals of a Jahn-Teller active intermediate

Zeineb Basdouri[a,b], Larry R. Falvello[b,*], Mohsen Graia[c], Milagros Tomás[d,*]

[a] Laboratoire de Matériaux, Cristallochimie et Thermodynamique Appliquée, Département de Chimie, Faculté des Sciences de Tunis, Université de Tunis El Manar, El Manar II, Tunis 2092, Tunisia
[b] Instituto de Nanociencia y Materiales de Aragón (INMA), Departamento de Química Inorgánica, CSIC-Universidad de Zaragoza, Zaragoza 50009, Spain
[c] Solid State Laboratory, Faculty of Sciences, University of Sfax, 1171, Sfax 3000, Tunisia
[d] Department of Inorganic Chemistry, Institute for Chemical Synthesis and Homogeneous Catalysis (ISQCH), CSIC-University of Zaragoza, Pedro Cerbuna, 12, Zaragoza 50009, Spain

ARTICLE INFO

Article history:
Received 1 September 2021
Revised 29 September 2021
Accepted 30 September 2021
Available online 3 October 2021

Keywords:
Reactive intermediate
Copper complex
Jahn-Teller
Ligand-field stabilization energy
Crystal-to-crystal transformation

ABSTRACT

Isolable crystals of the cesium salt of an anionic Jahn-Teller-active Cu complex, initially formed by reaction in solution, are spontaneously consumed in a solvent-mediated crystal-to-crystal transformation that produces a final product with a four-coordinate Cu center. Depending on the size of the crystals of the intermediate and the evaporation rate of the solvent, the transformation from intermediate to final product occurs in a two-week time frame. The crystalline Jahn-Teller Cu intermediate presents a noteworthy difference in stability compared to its non-Jahn-Teller Ni-centered isomorph. It is proposed that a Jahn-Teller intermediate may precede the formation of other four-coordinate Cu complexes.

1. Introduction

Any of a host of motivations can raise interest in characterizing transformations among crystalline solids, whether these be direct transitions or transformations enabled by another medium, usually solvent.

When only a single chemical species is involved, the key phenomenon is polymorphism, in which the species under consideration can exist in more than one crystalline form. If a single chemical species can crystallize in different forms with different minor coformers, such as solvent molecules, the phenomenon is solvatomorphism, which has also been called pseudopolymorphism. The kinetics of transformations involving polymorphs, if slow enough, may lead to the simultaneous presence of more than one form, designated as concomitant polymorphs. In all cases, polymorphs of whichever category are crystalline solids [1]. Studies of these phenomena, which have possible applications and implications in important areas, among them pharmaceuticals, mosquito-borne disease control [2] and agrochemicals, have been varied and nuanced.

Parallel considerations are pertinent to solid-state transformations that involve chemical reactions, in which bonds are formed and/or broken, but which proceed along a reaction coordinate that involves more than one chemical species and indeed may also include the formation of polymorphs if multiple solid products of a given species are involved. If a solid product of a chemical reaction is consumed in a subsequent transformation that takes place in contact with the original reaction medium, the full nature of the two-step process can escape observation; and the intermediate may disappear in favor of the final product. In such a case not only does a new species go uncharacterized (with the consequent loss of any potential applications or other interest that the species might possess), but in addition the full nature of the process that produces the final product is not correctly identified.

In what follows we report the reaction of the ligand orotate with a copper (II) starting material in aqueous solution, followed by evaporation to form a crystalline precipitate containing a six-coordinate, anionic Cu(II) complex (**1**) which, upon slight further evaporation of the solvent reacts spontaneously by loss of two coordinated water molecules to form a second crystalline product (**2**).

* Corresponding authors.
E-mail addresses: falvello@unizar.es (L.R. Falvello), milagros@unizar.es (M. Tomás).

https://doi.org/10.1016/j.molstruc.2021.131640

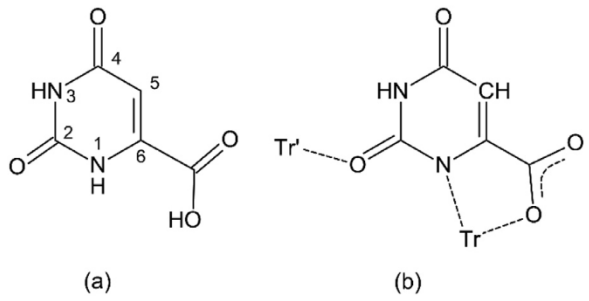

Fig. 1. (a) Orotic acid; (b) Example of orotate= coordination.

Intermediate **1** is sufficiently long-lived under its supernatant reaction solution to permit crystals to be harvested for analysis. In the analogous system with Ni(II) instead of Cu(II), reported previously [3], the product formed is isomorphous to **1** but undergoes no further reaction under similar conditions, either in solution or in the solid state.

The ligand employed in this study, orotate, is doubly deprotonated orotic acid (orotic acid, or H2orot, is 2, 4-dioxo-1H-pyrimidine-6-carboxylic acid, $C_5H_4N_2O_4$), Fig. 1a. Orotic acid is biologically important as a precursor in pyrimidine nucleobase synthesis [4]. While it is synthesized in the human body as part of that process, dietary consumption through cow's milk and root vegetables is also an important source for humans [5]. Our own interest in orotic acid and its deprotonated forms arises from the six functional groups at its periphery, which endow this species with the capacity to bind to transition metals in numerous modes [6], for instance as in Fig. 1b, while at the same time forming directed, and potentially structure-directing non-covalent interactions with its surroundings in crystalline solids [3,7].

2. Experimental

2.1. Materials and methods

Orotic acid monohydrate ($C_5H_4O_4N_2{\cdot}H_2O$), copper (II) carbonate ($CuCO_3$) and CsOH were obtained from commercial sources and were used without further purification. The nickel analogue $Cs_2[Ni(orot)_2(H_2O)_2]{\cdot}4H_2O$ (**3**) was prepared as described elsewhere [3]. The IR spectrum of newly prepared **3** is shown in Fig. S1 of the supporting information.

Infrared spectra were recorded on a Perkin-Elmer Spectrum 100 FT-IR spectrometer in the range of 4000–250 cm^{-1} using the ATR technique. Thermal analysis by TGA and DTA was performed using a TA Instruments STD-2960 at a heating rate of 10°C per min in a nitrogen atmosphere.

Synthesis of $Cs_2[trans\text{-}Cu(orot)_2(H_2O)_2]{\cdot}4H_2O$ (**1**) and $Cs_2[Cu(orot)_2]{\cdot}3H_2O$ (**2**).

An aqueous suspension of $CuCO_3$ (0.272 g, 2.20 mmol) and orotic acid monohydrate ($C_5H_4O_4N_2{\cdot}H_2O$; 0.76 g, 4.4 mmol) were stirred for 2 days in air allowing gas evolution; then a 0.39 M solution of CsOH (4.4 mmol, 11.28 ml) was added, and after two hours of stirring the resulting suspension was filtered and the blue solution was left standing for evaporation. After several days, some pale blue transparent blocks of compound **1** were observed inside the partially evaporated solution. Some of the blocks were removed from the solution and kept in a vial. It was observed that they become opaque with time (**1**; *vide infra*). Further evaporation of the remaining solution produced small darker blue crystals of **2** while the pale blue blocks of **1** disappeared. IR cm^{-1}: for compound **1**: 3574, 3088, 3003, 1622, 1360, 1018, 768, 542, 442, 418, Fig. S2; for solid **1´**: 3167, 3086, 1664, 1614, 1362, 1325, 1018, 1018, 808, 769, 445, Fig. S3; for compound **2**: 3460, 1624, 1361, 1320, 1021, 800, 771, 450, 327, Fig. S4.

2.2. Single-crystal X-ray structure determination of compounds *(1)* and *(2)*

Single-crystal diffraction data were measured using a Rigaku Oxford Diffraction Xcalibur S3 four-circle diffractometer equipped with graphite-monochromated Mo Kα radiation (λ = 0.71073 Å). Multi-scan corrections were applied to the data. Full crystallographic information for the structure analyses can be found in the CIF, which also contains embedded refinement instructions and diffraction data. Crystal data for **1**, CCDC number 2099291, $C_{10}H_{16}Cs_2CuN_4O_{14}$, M = 745.63, triclinic, a = 7.34016 (15), b = 8.59463(17), c = 9.33808(16) Å, α = 105.1804 (16), β = 101.5250 (16), γ = 110.9880 (19), U = 501.860 (18) $Å^3$, T = 173 (2) K, space group P(−1) (no. 2), Z = 1, 31,002 reflections measured, 3348 unique (R_{int} = 0.0424), all of which were included in the refinement. The final wR(F^2) was 0.0494 (all data). For **2**, CCDC number 2,099,292, $C_{10}H_{10}Cs_2CuN_4O_{11}$, M = 691.58, triclinic, a = 8.2822 (3), b = 9.4359 (3), c = 11.6315 (3) Å, α = 79.047 (3), β = 74.014 (3), γ = 75.444 (3), U = 838.63 (5) $Å^3$, T = 103 (2) K, space group P(−1) (no. 2), Z = 2, 15,618 reflections measured, 4005 unique (R_{int} = 0.0440), all of which were included in the refinement. The final wR(F^2) was 0.0776 (all data). Data collection and reduction: CrysAlisPro [8]. Structure solution: ShelxT [9]. Structure refinement: ShelxL [10]. Graphics: Mercury [11], Diamond [12].

For **2** a positive difference peak near Cs1 was interpreted as a minor disorder component, Cs1B. Correlation obviated an attempt to refine the relative occupancies of the two congeners. So single-point refinements were carried out for major-component occupancies of 0.50, 0.67, 0.75, 0.90 and 1.00, and with total occupation of the site held at 1.00. Similar residuals resulted in all cases tested except for 0.50, for which the refinement was unstable. For the final refinement the site-occupation factor for Cs1 was set to 0.75, the anisotropic displacement parameters for Cs1 and Cs1B were held equal, and a weak anti-bumping restraint was applied.

3. Results and discussion

3.1. Synthesis of $Cs_2[trans\text{-}Cu(orot)_2(H_2O)_2]{\cdot}4H_2O$ *(1)* and $Cs_2[Cu(orot)_2]{\cdot}3H_2O$ *(2)*

The reaction of $CuCO_3$, orotic acid monohydrate and CsOH in a 1:2:2 ratio in water yields an insoluble pale blue solid in an aqueous blue solution. The insoluble solid is removed by filtration and pale blue blocks of **1** can be obtained from the partial evaporation of that solution. If the blocks of **1** are left in contact with the solution while solvent evaporation continues, small darker blue crystals of a new compound (**2**), appear. Fig. 2 presents a photo of the aqueous solution, in which two large pale blue crystals of compound **1** and small crystals of compound **2** can be seen. At this point, compound **1** and compound **2** coexist beneath the same supernatant solution and they can be considered concomitant products. However, when that solution is left open to the air for further evaporation, the large blue crystals disappear while the quantity of the small, darker crystals increases, which establishes that the formation of **2** is a solvent-mediated crystal to crystal evolution from compound **1**. In fact, the result depends on the speed of the evaporation of the solvent. Since the process requires the presence of solvent, fast evaporation of the solvent will likely produce a mixture of **1** and **2**. Besides the difference in color and shape of crystals of compounds **1** and **2**, they can also be distinguished by their stability in air, since **1** loses its crystallinity in the absence of the mother liquor, forming **1'** (*vide infra*). The crystallinity of **1** cannot be recovered by addition of water to **1'**.

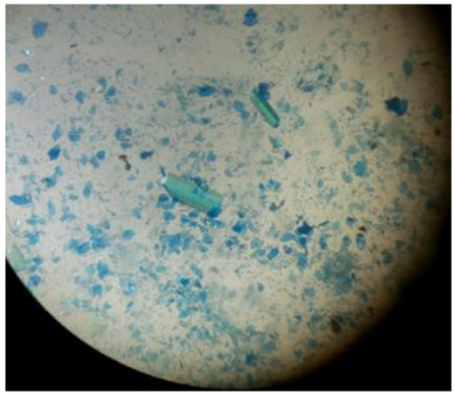

Fig. 2. Large crystals of compound **1** and small crystals of **2** below their supernatant solution. Fig. S8 is a photo of a solution from a separate preparation, with only crystals of compound **1**, before crystals of **2** began to form.

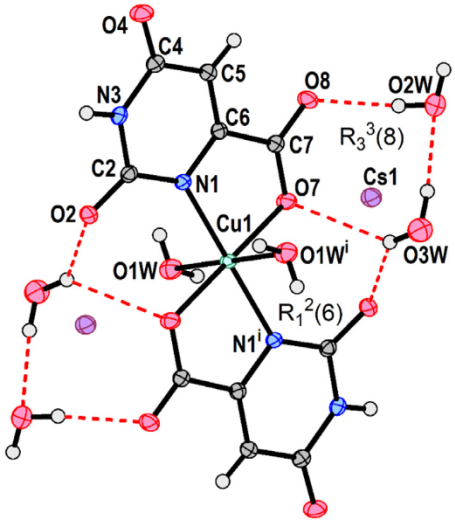

Fig. 3. One stoichiometric unit of Cs_2 [*trans*-Cu(orot)$_2$(H$_2$O)$_2$]·4H$_2$O, **1**. Non-H atoms are represented by their 50% probability ellipsoids. Symmetry code: (i) 1-x, 1-y, 1-z.

3.2. Structure and crystal stability of Cs_2[trans-Cu(orot)$_2$(H$_2$O)$_2$]·4H$_2$O (**1**). Solvent-mediated formation of Cs_2[trans-Cu(orot)$_2$]·3H$_2$O (**2**)

The crystal structure of compound **1** is formed by [*trans*-Cu(orot)$_2$(H$_2$O)$_2$]$^{(2-)}$ anions, Cs^+cations and unligated water molecules in a 1:2:4 ratio. The mononuclear anionic complex, Fig. 3, resides on a crystallographic inversion center and is formed by two chelating doubly deprotonated orotate ligands, trans to each other in the equatorial plane, and two apical aqua ligands. The orotate groups coordinate copper in the common chelate form through pyrimidine N1 and carboxylate O7 (Fig. 3). The apical aqua ligands, with Cu1-O1W 2.4650 (17) Å and ΔMSDA 0.0040 (7) Å^2, evince a static Jahn-Teller effect with a Jahn-Teller radius of 0.550 Å [13]. The J-T radius R_{JT} is defined by the relation $R_{JT}^2 = \sum_{i=1}^{6} \Delta d_i^2$, in which R_{JT} is the JT radius, the summation is over the six metal-ligand bonds, and Δd_i is the deviation of the *i*th M-L bond length from the mean of the six.

The coordination linkage from N1 to Cu1 shows significant misdirected valence (mdv), which can be quantified as the angle between the Cu1-N1 bond and the external bisector of the angle C2-N1-C6, Fig. S5; the latter in principle represents the axial direction of the σ orbital of N1. The mdv angle in **1** has a value of 13.8°.

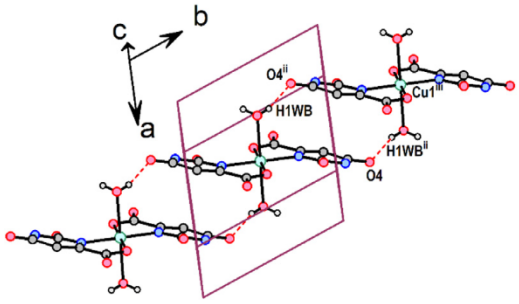

Fig. 4. Hydrogen-bonded chain of molecules of **1**, propagated parallel to the *b*-axis. Symmetry codes: (ii) 1-x, 2-y, 1-z; (iii) x, 1 + *y*, z.

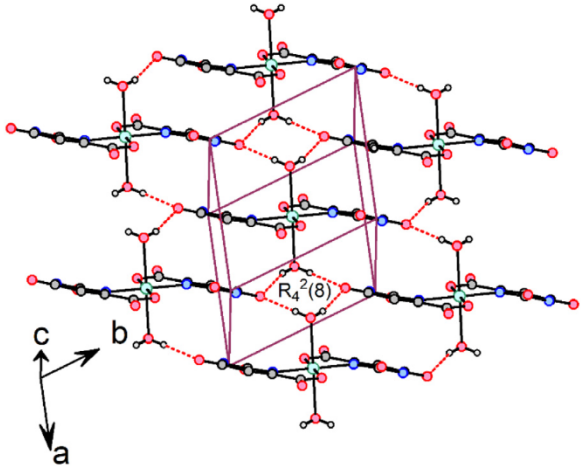

Fig. 5. Stacking of the chains in **1**, with successive chains linked at a four-molecule junction.

The dihedral angle between the plane of the carboxylate fragment C7/O7/O8, and the pyrimidine ring is 11.1 (2)°. The chelate angle N1-Cu1-O7 is 82.34 (6)°, adding a rhombic distortion in the equatorial plane to the axial Jahn-Teller distortion.

The two unligated water molecules at O2W and O3W, along with their inversion-related congeners, complete what can conveniently be regarded as the basic structural building block, Fig. 3. Together with the anionic complex, O2W and O3W complete a more regularly shaped fragment whose corners are filled by hydrogen-bonded $R_1^2(6)$ and $R_3^3(8)$ rings. Hydrogen bond geometry is collected in Table S1. A chain of complex anions extends parallel to the crystallographic *b*-axis, bound through O1W-H1WB...O4^{ii} H-bonds from the axial aqua ligand at O1W of the reference asymmetric unit to carbonyl group O4^{ii} (ii: 1-x, 2-y, 1-z) of the molecule centered at (x, 1 + *y*, z). This self-complementary interaction, completed by the H-bond O1W^{ii}-H1WB^{ii}...O4, Fig. 4, forms a ring with graph set symbol [14,15] $R_2^2(16)$, sitting astride inversion centers at (1/2, *n*, 1/2), where *n* is an integer.

These chains of anions, extending along the *b*-axis direction, are stacked upon each other in the *a*-axis direction, giving a two-dimensional hydrogen-bonded net parallel to the *ab*-plane and centered at *z* = 0.5. Successive chains in this net are joined at hydrogen-bonded four-molecule junctions with graph set symbol $R_4^2(8)$, Fig. 5. Axial aqua ligands of two of the molecules are involved, along with carbonyl O atoms O4 of the other two molecules at the junction. These junctions reside about crystallographic inversion centers located at (*n*, 1/2, 1/2), where *n* is an integer.

The space between the anionic *ab*- layers is estimated to be 148.5 Å^3 [16] which accounts for 29.6% of the unit-cell volume, and is occupied by Cs+ cations and free water molecules, Fig. 6. Cs1 is

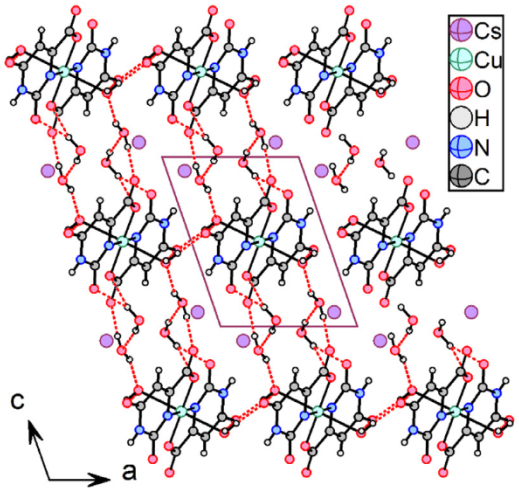

Fig. 6. Packing in the structure of **1**, with Cs+ lying in the space between *ab*-layers of the anionic complex.

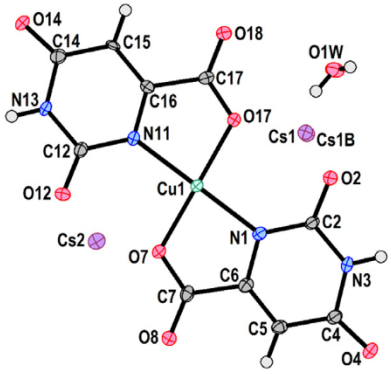

Fig. 7. The complex anion in Cs_2[*trans*-Cu(orot)$_2$]·3H_2O **2**, along with the Cs+ sites and one free water molecule. Disordered H_2O are not shown. Non-H atoms are represented by their 50% probability ellipsoids.

surrounded by eight oxygen atoms, congeners of carbonyl O atoms O2 (x2) and O4, carboxylate O atoms O7 and O8 (x2), and free water O3W (x2). Three more O atoms, farther away from Cs1, were not considered in this context on the grounds that they are bonded to H atoms that lie closer to Cs1 than do the O-atoms. The eight O atoms that we consider here form an irregular dodecahedron, Fig. S6, whose continuous shape measures [17] with respect to eight idealized polyhedra considered by the program SHAPE [18] are all greater than 10%. We thus do not venture to assign a name or symmetry to this polyhedron. A zig-zag chain of edge-sharing polyhedra runs parallel to the b-axis, incorporating as vertices O atoms from successive chains of anions, thus adding to the stability of the 2-D net parallel to the *ab*-plane.

When left beneath the aqueous solution from which they had crystallized, and with slow evaporation of that solution, crystals of **1** undergo a solvent-mediated transformation to Cs_2[*trans*-Cu(orot)$_2$]·3H_2O, **2**, in which the original complex is seen to have lost its two axial aqua ligands. Compound **2** is equivalent in connectivity, and similar in shape, to the equatorial plane of compound **1** – that is, a Cu (II) center on a general position is chelated by two orot$^{(2-)}$ ligands trans to each other, Fig. 7, giving a distorted square planar complex [chelate angles N1-Cu1-O7 82.86(13), N11-Cu1-O17 82.13(13)^0]. While the bond distances and angles that are common to **1** and **2** are quite similar, the subtleties of the molecular shape are different. The misdirected valence in **1** (13.8°) is the result of a tilting of the pyrimidine ring out of the equatorial coordination plane (pitch distortion, Fig. S5), whereas the mdv found

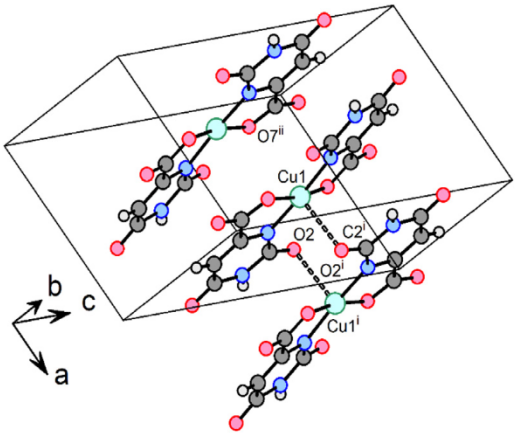

Fig. 8. Stacking of the anions in **2**, with O2^i and O7^{ii} in the nominally empty fifth and six coordination sites of Cu1. Symmetry codes: (i): 2-x, 1-y, 1-z; (ii) 1-x, 1-y, 1-z.

in **2** is of lesser magnitude (9.95 and 9.07° at N1 and N11, respectively) and corresponds to an in-plane rotation of each pyrimidine ring (yaw distortion, Fig. 7).

The orotate ligands in **2** are essentially flat, with the ring and carboxylate planes forming torsion angles N1-C6-C7-O7 and N11-C16-C17-O17 of −1.3(6)° and −1.9(6)°, respectively. The two *trans*-orotate ligands in **2** are not strictly coplanar, forming a dihedral twist angle of 14.24(9)°.

A fifth potential coordination site in **2** is occupied by O2^i of the molecule at (2-x, 1-y, 1-z), with Cu1...O2^i = 2.588 (3) Å (Fig. 8). We do not represent this contact as a full-fledged coordination bond, on the basis of two considerations. Firstly, in the absence of a sixth ligand the long M-O distance cannot be attributed to the Jahn-Teller effect. Secondly, the Cu1...O2^i-C2^i angle of 106.7 (3)° and especially the fact that the plane formed by these three atoms contains the π electron density of the carbonyl group C2^i-O2^i, signify that the main overlap in this interaction is between the $d(z^2)$ orbital of the metal and the π electron density at O2^i, an unsymmetrical overlap to which we do not attribute a significant degree of covalency.

Opposite O2^i, in what would be a sixth coordination site around Cu1, the nearest atom to Cu1 is O7^{ii} of the molecule at (1-x, 1-y, 1-z), with Cu1...O7^{ii} = 3.423 (3) Å and O2^i...Cu1...O7^i = 173.08 (8)°. Cu1...O7^{ii} is typical of the long axial contacts seen in crystal structures of square-planar transition metal complexes (Fig. 8).

The complex anion forms a chain parallel to the direction [1,0,-1], mediated by self-complementary H-bonded $R_2^2(8)$ interactions involving N3/H3 and O4 of one molecule and N13/H13 and O14 of the next molecule along the chain (Fig. 9). The chains are stacked along the [100] direction, with stability derived from the contacts involving the formally empty fifth and sixth coordination sites of Cu, as described above (Fig. 8). The combined formation of chains along [1,0,-1] and stacking along [100] yields a 2D net parallel to the (010) plane, centered at $y = n + 0.5$, where n is any integer (Fig. 10). The spaces between these layers are occupied by the Cs^+ cations and uncoordinated water molecules, including a zig-zag chain of four partially occupied water sites per asymmetric unit, propagated parallel to the *a*-axis (Fig. 10). The final refined model for **2** describes a stoichiometry with three uncoordinated water molecules per copper complex. One fully occupied free water and its congeners are situated in pairs about inversion centers at (0, 0, 1/2) and lattice-related positions.

*Compound **1** undergoes water loss when left in the laboratory atmosphere.* When crystals of six-coordinate complex **1** are left at ambient conditions, without the solvent from which the crystals

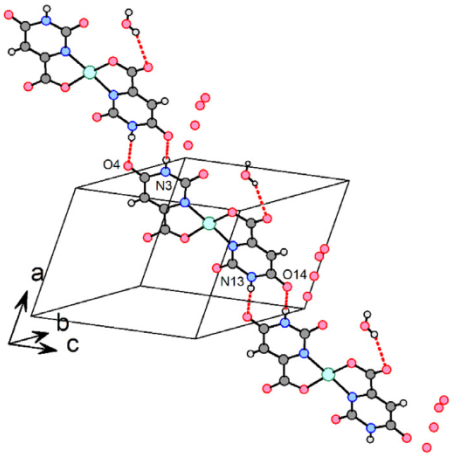

Fig. 9. In the structure of **2**, chains of anions propagated along [1,0,-1], mediated by self-complementary H-bonding interactions.

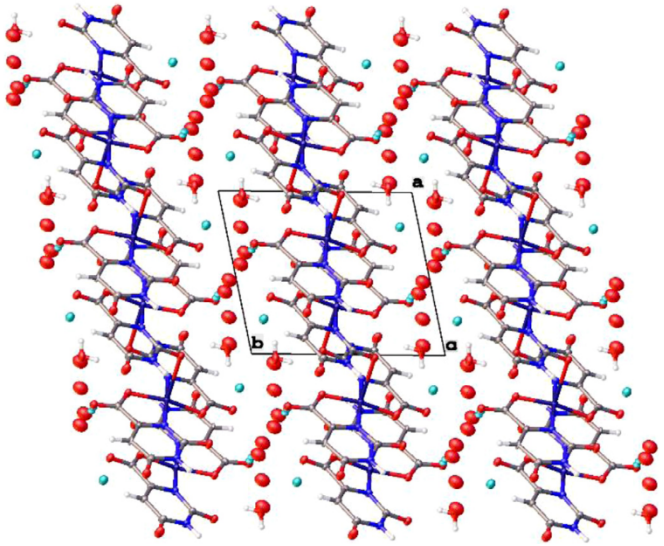

Fig. 10. Two-D nets of anions parallel to (010) in the structure of **2**. Non-H atoms are drawn at the 50% probability level in order to portray the systematically larger ellipsoids for the chains of partially occupied free water sites.

had grown, they are seen to deteriorate, taking on an opaque appearance. This occurs in open air and also when the crystals are stored without solvent in a closed vial. A new solid is formed, which we call **1′**. In the absence of accurate structural characterization, we conclude from the available data that **1′** maintains the ionic nature seen for **1**, with loss of both coordinated and uncoordinated water. Importantly, the sample of **1′** thus formed does not regain the original crystallinity of **1** upon exposure to water.

The IR spectrum of the opaque crystals of **1'** (Fig. S3) shows better defined (less broad) absorptions than those seen for the crystalline forms of **1**, and fewer and smaller absorptions in the OH region, which suggests that the loss of crystallinity occurs by water egress. By way of reaching a formulation for **1′**, we consider the TGA/DTA measurements obtained from **1′** and **3**, the nickel complex that is isostructural to Cu compound **1** (*vide infra*). As seen in Fig. 11, the TGA/DTA show weight loss below 200 C for both **1′** (blue in the figure) and **3** (red). We interpret this weight loss as involving only water in both cases. It is clear that at the outset of the TGA measurements, Ni compound **3** contains more water than does **1′**. For Cs_2[*trans*-Ni(orot)$_2$(H_2O)$_2$]·4H_2O the total water mass is 14.6%; the measured loss is 14.10%. For **1′**, formed when **1** (isostructural with **3**) loses water, the weight loss is 3.9%. The calculated weight loss for a sample beginning with stoichiometry corresponding to Cs_2[*trans*-Cu(orot)$_2$]·1.5H_2O would be 4.1%. The temperature at which weight loss occurs for Ni-containing **3**, 130 C, is also higher than that for the partially dehydrated Cu compound **1′**, 81 C.

*Comparison of compound **1** with its Ni-centered isomorph, **3**.* The Ni-centered analogue of Cu-based compound **1** was reported some years ago (CSD deposition number 649149) [3]. The two structures are almost identical (Fig. S7a), with the only significant difference being the axial M—OH_2 bond distance, which is longer in the Cu Complex **1** as a result of static Jahn-Teller elongation. The obvious question is why the Cu compound undergoes further change under ambient conditions-either progressive decomposition in the absence of water or solvent-mediated transformation in its presence. The crystal-to-crystal transformation involves loss of the axial water, and the evidence is strong that the decomposition at ambient conditions involves the same axial water loss. The fact that the Ni-centered complex does not undergo these changes under the same conditions provides an enigmatic counterpoint to the behavior of the Cu complex, especially given that the two are isomorphous.

In seeking an explanation for these different behaviors, we consider both molecular and crystal-based factors. In terms of the crystal, compounds **1** and **3** both have the same rich network of hydrogen bonds, with each of the three independent water fragments acting as donor in two such interactions. The geometric parameters of the corresponding H-bonds in the two structures are remarkably similar, even for those involving the axial water ligand O1W in **1** (Table S1). Despite a difference in temperature for the two determinations-**1** and **3** were measured at T = 173(2) and 100(1) K, respectively -their extended structures can be overlaid very closely (Fig. S7b).

That compound **1** proceeds to compound **2** may be attributed in part to differences in crystal stability, but we see that as a tenuous explanation at best for the difference in this regard between **1** and **3**. To the extent that water content may be important, the presence of a total of six coordinated and free water molecules per Cu in **1** can be contrasted to the three waters per Cu present in **2**. We cannot give a concrete analysis of the H-bonding in **2** because of the five free water sites; four of them are partially occupied and their H atoms have not been located. We have observed no sign that compound **3** evolves to a nickel-centered analogue of **2** or to another product. It is thus worthwhile at least to consider factors arising from the nature of the molecules.

Considering factors intrinsic to the molecules themselves, the clear difference between **1** and **3** is that the axial aqua ligands are not as firmly anchored to Cu as to Ni. The Jahn-Teller effect is inherently dynamic and can be a possible disruptive factor in **1**. Beyond that, we can appeal to ligand field stabilization energy for a simple explanation of the different behaviors of the Cu and Ni complexes. As was explained as early as 1952 by Orgel [19], considering only ground-state electronic configurations, when a Cu(2+) center, with its lone electron hole, undergoes transition from octahedral to square-planar coordination, the electron hole migrates to the plane of the four remaining ligands, occupying the higher energy $d\ (x^2\text{-}y^2)$ orbital along with one electron, while the remaining pair of $e(g)$ electrons occupy $d(z^2)$. The half-empty $d\ (x^2\text{-}y^2)$ orbital imparts at least some stability to the new planar arrangement. This advantage is not shared by Ni (2+), which has single electron holes in each of the two e (g) orbitals. Thus, for the Ni complex the ligand-field splitting consequent to the elongation of the bonds to the two axial ligands would stabilize one of the e (g) orbitals and destabilize the other to the same extent. This elongation would have to continue until the orbital energy difference reached parity with the electron pairing energy, in order for the

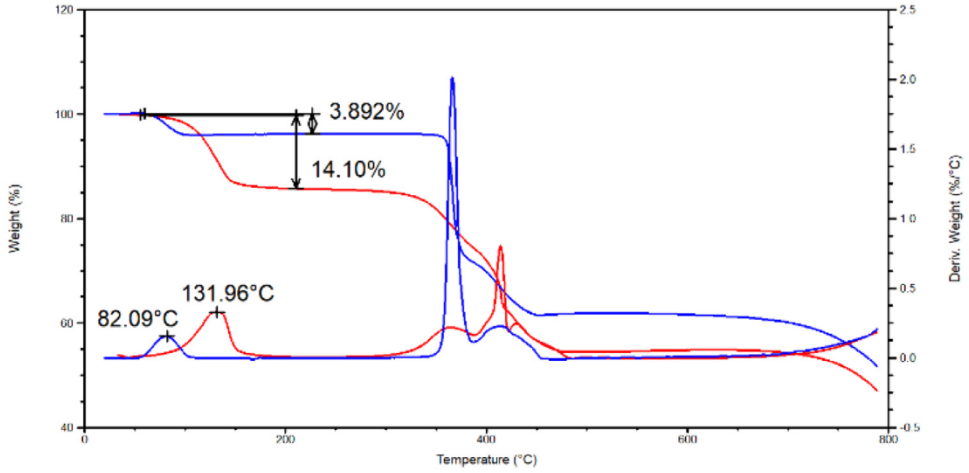

Fig. 11. TGA weight loss and the derivative of weight loss for compounds **1′** (blue traces) and **3** (red).

transition to take place. This may offer some insight into the different behaviors that we observe for the isostructural octahedral Cu (2+) and Ni (2+) complexes **1** and **3**; and this is not intended to overlook the well-known stability of square-planar, diamagnetic Ni (2+) complexes, in which an empty excited-state orbital is strongly stabilized.

4. Conclusion

Crystals of Jahn-Teller-active compound **1** are labile both in a laboratory atmosphere and beneath an aqueous solution, evolving to a crystalline solid with a lesser ratio of water to Cu. The fact that the isostructural Ni-containing crystals do not undergo any change under analogous conditions suggests that an explanation of the behavior of the Cu system extends beyond considerations of the packing and intermolecular forces in the crystal. Crystal field stabilization energy is a possible contributor to the difference in these two molecular crystalline systems. Whatever the case may be in that regard, the isolation of compound **1** suggests that the preparation of the far more frequently isolated four-coordinate Cu(II) complexes may involve a hexacoordinated Jahn-Teller-active Cu(II) compound as a disappearing intermediate.[1] This in turn raises the intriguing possibility that there are heretofore unobserved Jahn-Teller compounds – intermediates in the formation of four-coordinate Cu complexes – that still await discovery.

Funding

This work was supported by the Spanish Ministerio de Ciencia e Innovación (Grant PGC2018–093451-B-I00), the European Union Regional Development Fund, (FEDER), and the Diputación General de Aragón, Project M4, E11_20R. The authors acknowledge the use of the Servicio General de Apoyo a la Investigación-SAI, Universidad de Zaragoza.

Supplementary crystallographic data: CCDC 2099291 and 2099292 contain the supplementary crystallographic data for this paper. These data can be obtained through doi:http://www.ccdc.cam.ac.uk/conts/retrieving.html or from the Cambridge crystallographic data center, 12, Union Road, Cambridge CB2 1EZ, UK; fax: +44 1223 336,033.

[1] A search of the Cambridge structural database version 2020.3.0 [20], retrieves 4603 entries for four-coordinate Cu with an N_2O_2 ligand set (Cu—L distances between 1.8 and 2.2 Å). A search for the same fragment but with two mutually *trans*- axial oxygen-bound ligands (Cu—O_{ax} 2.3–2.8 Å) yields 1578 entries. A similar search for Ni complexes, with all distances in the range 1.8–2.2 Å, yields 1711 four-coordinate- and 2921 six-coordinate complexes.

Declaration of Competing Interest

There are no conflicts to declare.

Supplementary materials

Supplementary material associated with this article can be found, in the online version, at doi:10.1016/j.molstruc.2021.131640.

CRediT authorship contribution statement

Zeineb Basdouri: Conceptualization, Validation, Investigation, Writing – review & editing. **Larry R. Falvello:** Conceptualization, Validation, Formal analysis, Investigation, Data curation, Writing – original draft, Funding acquisition. **Mohsen Graia:** Conceptualization, Investigation, Writing – review & editing, Supervision. **Milagros Tomás:** Conceptualization, Investigation, Formal analysis, Writing – review & editing, Funding acquisition.

References

[1] J. Bernstein, Polymorphism in molecular crystals, Polymorph. Mol. Cryst. (2010) 1–424 9780199236565, doi:10.1093/ACPROF:OSO/9780199236565.001.0001.
[2] J. Yang, B. Erriah, C.T. Hu, E. Reiter, X. Zhu, V. López-Mejías, I.P. Carmona-Sepúlveda, M.D. Ward, B. Kahr, A deltamethrin crystal polymorph for more effective malaria control, Proc. Natl. Acad. Sci. U S A. 117 (2020) 26633–26638, doi:10.1073/pnas.2013390117.
[3] L.R. Falvello, D. Ferrer, M. Piedrafita, T. Soler, M. Tomás, Using the crystal to engineer the molecule: Cis-*trans*-isomer selection in anionic bis(orotate) complexes, CrystEngComm 9 (2007) 852–855, doi:10.1039/b709168k.
[4] M. Löffler, L.D. Fairbanks, E. Zameitat, A.M. Marinaki, H.A. Simmonds, Pyrimidine pathways in health and disease, Trends Mol. Med. 11 (2005) 430–437, doi:10.1016/j.molmed.2005.07.003.
[5] M. Löffler, E.A. Carrey, E. Zameitat, Orotic Acid, More than just an intermediate of pyrimidine de novo synthesis, J. Genet. Genom. 42 (2015) 207–219, doi:10.1016/j.jgg.2015.04.001.
[6] C.P. Raptopoulou, V. Tangoulis, V. Psycharis, Synthesis and structural, spectroscopic, and magnetic characterization of $(NH_4)[Fe_3(\mu\text{-}OH)(H_2L)_3\ (HL)_3]$ (H_3L = Orotic acid) presenting two novel metal-binding modes of the orotate ligand, Inorg. Chem. 39 (2000) 4452–4459, doi:10.1021/ic9914084.
[7] I. Ara, Z. Basdouri, L.R. Falvello, M. Graia, P. Guerra, M. Tomás, Tetra-*n*-butylammonium orotate monohydrate: knowledge-based comparison of the results of accurate and lower-resolution analyses and a non-routine disorder refinement, Acta Crystallogr. Sect. E Crystallogr. Commun. 75 (2019) 1632–1637, doi:10.1107/S2056989019013380.
[8] CrysAlisPro 1.171.39.44a. Rigaku Oxford Diffraction, Yarnton, Oxfordshire, England, 2018.

[9] G.M. Sheldrick, SHELXT - Integrated space-group and crystal-structure determination, Acta Crystallogr. Sect. A Found. Crystallogr. 71 (2015) 3–8, doi:10.1107/S2053273314026370.
[10] G.M. Sheldrick, Crystal structure refinement with SHELXL, Acta Crystallogr. Sect. C Struct. Chem. 71 (2015) 3–8, doi:10.1107/S2053229614024218.
[11] C.F. MacRae, I. Sovago, S.J. Cottrell, P.T.A. Galek, P. McCabe, E. Pidcock, M. Platings, G.P. Shields, J.S. Stevens, M. Towler, M. Towler, P.A. Wood, Mercury version 4.0., Mercury 4.0: from visualization to analysis, design and prediction, J. Appl. Crystallogr. 53 (2020) 226–235, doi:10.1107/S1600576719014092.
[12] K. Brandenburg Diamond version 4.6.4, Klaus Brandenburg, Crystal Impact GbR, Bonn, Germany, 2020.
[13] L.R. Falvello, Jahn-Teller effects in solid-state co-ordination chemistry, J. Chem. Soc. Daltons Trans. (1997) 4463–4475, doi:10.1039/a703548i.
[14] M.C. Etter, Encoding and decoding hydrogen-bond patterns of organic compounds, Acc. Chem. Res. 23 (1990) 120–126, doi:10.1021/ar00172a005.
[15] J. Bernstein, R.E. Davis, L. Shimoni, N.L. Chang, Patterns in hydrogen bonding: functionality and graph set analysis in crystals, Angew. Chem. Int. Ed. 34 (1995) 1555–1573, doi:10.1002/anie.199515551.
[16] A.L. Spek, Platon, a multipurpose crystallographic tool., CheckCIF validation ALERTS: what they mean and how to respond, Acta Crystallogr. Sect. E Crystallogr. Commun. 76 (2020) 1–11, doi:10.1107/S2056989019016244.
[17] M. Pinsky, D. Avnir, Continuous symmetry measures. 5. The classical polyhedra, Inorg. Chem. 37 (1998) 5575–5582, doi:10.1021/ic9804925.
[18] M. Llunell, D. Casanova, J. Cirera, P. Alemany, S. Alvarez, SHAPE V2.1, Universitat de Barcelona, 2013.
[19] L.E. Orgel, The effects of crystal fields on the properties of transition-metal ions, J. Chem. Soc. (1952) 4756–4761, doi:10.1039/JR9520004756.
[20] C.R. Groom, I.J. Bruno, M.P. Lightfoot, S.C. Ward, The Cambridge structural database, Acta Crystallogr. Sect. B Struct. Sci. Cryst. Eng. Mater. 72 (2016) 171–179, doi:10.1107/S2052520616003954.